



Contents lists available at ScienceDirect

Journal of Rock Mechanics and Geotechnical Engineering

journal homepage: www.jrmge.cn

Full Length Article

Modelling gas diffusion in compacted water-saturated Na-bentonite considering multi-porosity effects

Linyong Cui ^{a,*}, Min Chen ^b, Zirui Cheng ^c, Shakil A. Masum ^d, Yanan Cui ^a^a Department of Civil and Environmental Engineering, The Hong Kong Polytechnic University, Hung Hom, Kowloon, 999077, Hong Kong, China^b Key Laboratory of Marine Geology, Tongji University, Shanghai, 200092, China^c Department of Civil Engineering, Nanjing University of Science and Technology, Nanjing, 210094, China^d Geoenvironmental Research Centre, Cardiff School of Engineering, Cardiff University, Cardiff, CF24 3AA, UK

ARTICLE INFO

Article history:

Received 28 July 2024

Received in revised form

3 January 2025

Accepted 13 January 2025

Available online xxx

Keywords:

Gas diffusion

Saturated bentonite

Montmorillonite

Interlayer pore

Tortuosity

ABSTRACT

Predicting the gas diffusion coefficient of water-saturated Na-bentonite is crucial for the overall performance of the geological repository for isolating high-level radioactive waste (HLW). In this study, a conceptual model that incorporates a multi-porosity system was proposed, dividing the pore space into free water pores, interlayer water pores, and diffuse double layer (DDL) water pores, to describe the molecular diffusion behaviour of the dissolved gas in saturated bentonite. In this model, gas diffusion in these three porosities is considered as independent and parallel processes. The apparent gas diffusion coefficient is quantified by applying weighted approximations that consider the specific porosity, tortuosity factor, and constrictivity factor within each porosity domain. For verification, experimental data from gas diffusion tests on saturated MX-80 and Kunipia-F bentonite specimens across a wide range of dry densities were utilized. The proposed model could successfully capture the overall trend of the apparent gas diffusion coefficient for bentonite materials across the partial dry density of montmorillonite ranging from 900 kg/m³ to 1820 kg/m³, by employing only one fitting parameter of the scaling factor. When the partial dry density of montmorillonite decreased to 800 kg/m³, the proposed model shows an underestimation of the apparent gas diffusion coefficient due to possible changes of the tortuosity factor. Model predictions indicate that gas diffusion in saturated bentonite is primarily controlled by the free pore domain, with minimal contributions from DDL pores. Despite being the dominant pore type, interlayer pores contribute limitedly to total D_a/D_w values due to significant constrictivity effects. © 2025 Institute of Rock and Soil Mechanics, Chinese Academy of Sciences. Published by Elsevier B.V. This is an open access article under the CC BY-NC-ND license (<http://creativecommons.org/licenses/by-nc-nd/4.0/>).

1. Introduction

Sodium bentonites, which are rich in Na-montmorillonite, are essential components in engineered barriers for the subsurface disposal of high-level radioactive waste (HLW) in deep geological repositories. This preference stems from their advantageous qualities, including low hydraulic conductivity, high adsorption capacity, and effective self-sealing properties (Bourg et al., 2007). Throughout the prolonged operation of a repository, gases such as hydrogen, methane, and carbon dioxide are inevitably produced through various mechanisms, such as organic matter degradation,

groundwater radiolysis, and anaerobic metal corrosion (Liu et al., 2020, 2024; Ni et al., 2023). During gas generation, the repository's near field is typically saturated with pore water, leading to the initial dissolution of generated gases into the pore water. The saturated hydraulic conductivity of the barrier materials generally remains in a lower level, which could ensure minimal advective transport of these dissolved gases, with molecular diffusion under concentration gradients emerging as the dominant mechanism for gas migration (Liu et al., 2021). Furthermore, if the gas generation rate surpasses the rate of gas diffusion into the bentonite barriers, a discrete gas phase may develop, potentially compromising the barrier performance. Therefore, accurate estimates of gas diffusion coefficients will be indispensable for determining an accurate and thorough equilibrium between gas generation and dissipation.

Over the past decades, efforts to anticipate how bentonite barriers will perform have prompted many investigations into gas

* Corresponding author.

E-mail address: linyong.cui@polyu.edu.hk (L. Cui).

Peer review under responsibility of Institute of Rock and Soil Mechanics, Chinese Academy of Sciences.

<https://doi.org/10.1016/j.jrmge.2025.01.044>1674-7755/© 2025 Institute of Rock and Soil Mechanics, Chinese Academy of Sciences. Published by Elsevier B.V. This is an open access article under the CC BY-NC-ND license (<http://creativecommons.org/licenses/by-nc-nd/4.0/>).

diffusion and flow behaviour within compacted saturated bentonites and other clay materials employed in disposal of nuclear waste (Eriksen and Jacobsson, 1982; Neretnieks, 1985; Sato et al., 2001; Higashihara et al., 2001, 2005; Jacops et al., 2017; Radeisen et al., 2023; Watanabe et al., 2023). Gas diffusion experiments typically involve measuring and interpreting concentration profiles within a clay specimen in relation to the apparent diffusion coefficient. Within the water-saturated bentonite, where montmorillonite predominates as the primary clay mineral, there exists a simultaneous presence of interlayer water, diffuse double layer (DDL) water and free pore water (Appelo et al., 2008). Typically, the pores containing free water contribute the most to the diffusion process, owing to their larger diameters compared to the DDL and interlayer pores. Based on systematic transient gas diffusion tests, Sato et al. (2001) reported that, both the pore water, where the mobility of water molecules is constrained near the montmorillonite surface, and the interlayer water within montmorillonite, could potentially serve as the media for the diffusional transport of dissolved gas. Nevertheless, the precise extent of each contribution remains unclear. Shackelford and Moore (2013) and Kant and Prerna (2022) noted reduced rates of diffusion of cations within the DDL near the montmorillonite surface compared to regions farther away. Molecular dynamics (MD) simulations further support this observation, indicating slightly lower mobility of water and cations within DDL water compared to free water (Rotenberg et al., 2007). The diffusion characteristics of interlayer water depend on the number of water layers present within the montmorillonite structure. Studies have shown that sodium in the 3-layer hydrate exhibits diffusion coefficients comparable to those of DDL water (Chang et al., 1995; Rotenberg et al., 2007). However, the diffusion coefficient of Na^+ appears to decrease significantly by 1 and 2 orders of magnitude for the 2- and 1-layer hydrate, respectively (Chang et al., 1995; Marry et al., 2002). Based on these experimental observations, certain diffusion models delineate the apparent diffusion coefficient into segments linked with free pore water, DDL water, and interlayer water (Bourg et al., 2006, 2007; Kozaki et al., 2008).

It should be noted that previous experimental investigations and theoretical models of solute diffusion have predominantly focused on both cations and anions in compacted bentonite (Van Loon et al., 2007; Bourg et al., 2007; Schampera et al., 2016; Geng et al., 2022; Kumar et al., 2023; Wu et al., 2023; Cui et al., 2024). However, gas diffusion in water differs significantly from those of cations. Experimentally, helium and hydrogen gases, classified as neutral species, are commonly employed as permeants for conducting gas diffusion and flow tests on bentonite materials (Sato et al., 2001; Higashihara et al., 2001, 2005; Cui et al., 2019, 2020, 2022). The diffusion coefficients of these gases can be higher than those of ions in a hydrated state (Sato et al., 2001). This discrepancy arises because helium and hydrogen gases diffuse within the unoccupied space among water molecules in their liquid state, contrasting with the diffusion of ions in the hydration state. Up to now, there is very limited availability of experimental studies for investigating the gas diffusion behaviour in water-saturated, compacted bentonite. This is because experimental measurement of the diffusion coefficient can be extremely time-consuming due to the presence of pores within compacted bentonite that can be as small as several nanometers. Furthermore, models for predicting the apparent diffusion coefficient of dissolved gases are even less reported in the literature.

In this study, we proposed a conceptual model that incorporates a multi-porosity system, dividing the pore space within saturated Na-bentonite into free water pores, DDL water pores and the interlayer water pores, to describe the gas diffusion behaviour.

Meanwhile, the apparent gas diffusion coefficient was quantified by applying weighted approximations that consider the specific porosity, tortuosity factor, and constrictivity factor within each porosity domain. Following this, we propose a methodology to ascertain these parameters based on the crystallographic information of montmorillonite minerals. Finally, comparisons and comprehensive evaluations between the model prediction results with experimental data are conducted. This approach could provide a novel perspective for understanding the molecular diffusion of dissolved gas in bentonite materials.

2. Model development

For a conservative, non-sorbing solute transport through a water-saturated homogenous porous medium, Sposito et al. (1979) reported that a macroscopic mass balance can be derived from the generalized Fick's law, incorporating a tensor of apparent diffusion coefficient, \mathbf{D}_a , which encompasses contributions from both hydrodynamic dispersion and molecular diffusion as

$$\frac{\partial C}{\partial t} = \nabla \cdot (\mathbf{D}_a \cdot \nabla C) - \mathbf{V} \cdot \nabla C \quad (1)$$

where C represents the solute concentration in the pore water and \mathbf{V} denotes the Darcy velocity vector. If the advective flow is neglected as compared to the molecule diffusion, the Darcy velocity can be overlooked and Eq. (1) can be given as

$$\frac{\partial C}{\partial t} = \frac{\partial}{\partial x_i} \left(D_{a,i} \frac{\partial C}{\partial x_i} \right) \quad (2)$$

where $D_{a,i}$ represents the apparent diffusion coefficient of the solute mass flux density associate with the x_i (principal axis) direction.

The fundamental concept underlying the gas diffusion model proposed in this study is to construct a multi-porosity system within saturated bentonite materials, comprising free water pores, DDL water pores, and interlayer water pores, as presented in Fig. 1. Within this system, the individual contributions of gas diffusion coefficients in the three types of porewater domains to the total diffusion coefficient can be determined based on microstructure information of montmorillonite.

Gas diffusion through a water-saturated specimen entails traversing an additional distance compared to diffusion in bulk water, because the dissolved gas molecule has to circumnavigate the soil particles. Boving and Grathwohl (2001) described diffusion coefficient as a function of effective transport porosity, tortuosity, and sorption. For porous media containing a significant fraction of nanopores, an additional parameter, the constrictivity factor, should be included. Therefore, the apparent diffusion coefficient of gas in Eq. (2) can be expressed as follows (Boving and Grathwohl, 2001; Bourg et al., 2006):

$$D_a = \frac{D_w \eta_e \delta}{(\eta + K_d \rho) \tau^2} \quad (3)$$

where D_w denotes the gas diffusion coefficient in bulk water (m^2/s); η_e and η represent the effective transport porosity and the total porosity, respectively; τ is the tortuosity, which is related to the ratio of the actual travel path length l_e within a porous medium to the straight-line distance l of the bentonite specimen ($\tau = l_e/l$); δ is the constrictivity, which measures the narrowing and widening of pores; K_d represents the distribution coefficient (m^3/kg); and ρ denotes the bulk density of the specimen (kg/m^3). Given that the

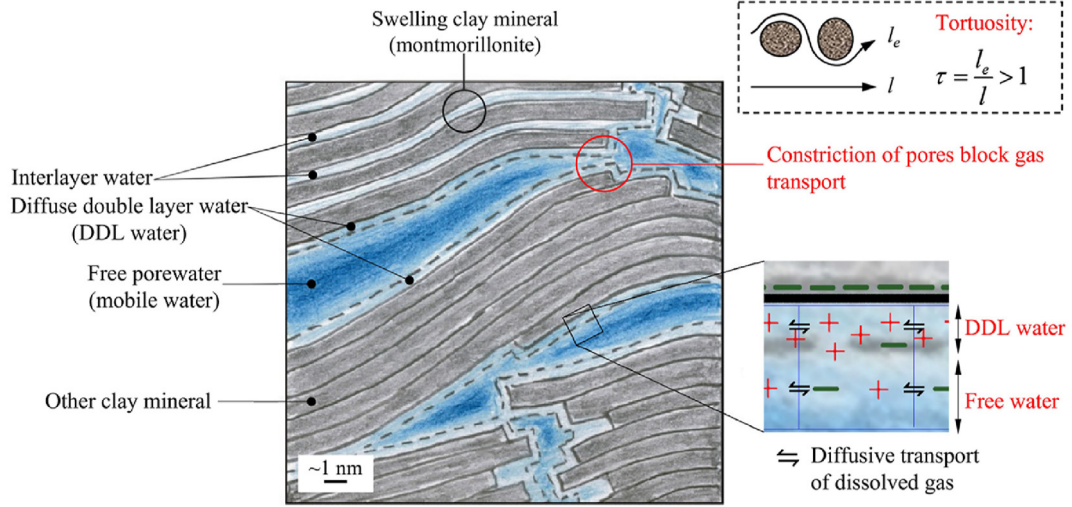


Fig. 1. Schematic diagram of molecular diffusion of gas within various types of porewater domains in saturated bentonites (adapted from Appelo et al. (2008)).

physical adsorption of helium and hydrogen gases on the montmorillonite is significantly weaker, the retardation of gases due to adsorption is considered negligible. Consequently, K_d is considered to be zero. Moreover, based on the assumption that the effective porosity is equal to the overall porosity, the apparent diffusion coefficient for non-sorbing dissolved gases can be given by (Sato et al., 2001; Cui et al., 2023):

$$\frac{D_a}{D_w} = \frac{\delta}{\tau^2} = \frac{\delta}{(l_e/l)^2} \quad (4)$$

In Eq. (4), the apparent diffusion coefficient of dissolved gas is only related with the ratio of δ/τ^2 , regardless of water types within the pore space of bentonite. However, in the case of saturated compacted bentonite, gas diffusion coefficient can vary among free water pores, DDL water pores, and interlayer water pores, as mentioned above. Therefore, it is essential to make a careful distinction between these three pore categories. Hueckel et al. (2018) once explained the impact of porewater types on clay swelling mechanics by differentiating the contributions of interlayer pores and larger pores. Therefore, in this study, we also conceptually divide the porosity in compacted, water-saturated bentonite into three categories: free water porosity, DDL water porosity, and interlayer water porosity, denoted by their respective values of η_{free} , η_{DDL} and η_{inter} :

$$\eta = \eta_{free} + \eta_{DDL} + \eta_{inter} \quad (5)$$

It is proposed that the diffusion process of dissolved gas in these three porosities can be described as separate and parallel processes, each characterized by its unique values of D_a/D_w , denoted as $(D_a/D_w)_{free}$, $(D_a/D_w)_{DDL}$, and $(D_a/D_w)_{inter}$, respectively. Moreover, the D_a/D_w of dissolved gas within compacted, water-saturated bentonite is considered as the weighted mean of D_a/D_w across the free, DDL, and interlayer pore domains, with each domain's contribution approximated by its respective porosity as follows:

$$\frac{D_a}{D_w} = \frac{\eta_{free}}{\eta} \left(\frac{D_a}{D_w} \right)_{free} + \frac{\eta_{DDL}}{\eta} \left(\frac{D_a}{D_w} \right)_{DDL} + \frac{\eta_{inter}}{\eta} \left(\frac{D_a}{D_w} \right)_{inter} \quad (6)$$

Using Eq. (4) to calculate $(D_a/D_w)_{free}$, $(D_a/D_w)_{DDL}$, and $(D_a/D_w)_{inter}$ from Eq. (6), the model expression for predicting apparent diffusion coefficient of dissolved gas can be obtained:

$$\frac{D_a}{D_w} = \frac{\delta_{free}}{\tau_{free}^2} \frac{\eta_{free}}{\eta} + \frac{\delta_{DDL}}{\tau_{DDL}^2} \frac{\eta_{DDL}}{\eta} + \frac{\delta_{inter}}{\tau_{inter}^2} \frac{\eta_{inter}}{\eta} \quad (7)$$

Obviously, the prerequisite for determination of D_a/D_w of saturated Na-bentonite is to ascertain the parameters of porosity η , constrictivity δ and tortuosity τ in the three types porewater domains.

2.1. Determination of porosity distribution in saturated bentonite

2.1.1. Interlayer porosity

On the length scale of tens of nanometers, montmorillonite particles in Na-bentonite materials are formed by parallel stacking an assemblage of tetrahedral-octahedral-tetrahedral (TOT) layers. Assuming the montmorillonite is homogeneous and the TOT layers are perfectly parallel, Kozaki et al. (2001) stated that the interlayer porosity η_{inter} could be computed based on the area of internal basal surface and the interlayer distance according to the following equation:

$$\eta_{inter} = \frac{A_{inter}}{2} h_{inter} \omega \rho_d \quad (8)$$

where A_{inter} is the area of internal basal surface of the TOT layer per unit mass of montmorillonite (m^2/kg), h_{inter} is the interlayer distance (m), ρ_d represents the dry density of bentonite materials (kg/m^3), and ω denotes the mass fraction of montmorillonite.

The clay crystal is made of unit-cells stacked in three dimensions with lateral dimensions given by: an_a , bn_b and cn_c . Therefore, internal basal surface area of montmorillonite per unit mass A_{inter} can be determined based on the dimensions of the unit-cell and the mass fraction of montmorillonite in bentonites, as in Tournassat et al. (2011):

$$A_{inter} = \frac{2(n_a a)(n_b b)(n_c - 1)}{n_a n_b n_c} \frac{N_A}{MW} = \frac{2ab(n_c - 1)}{n_c} \frac{N_A}{MW} \quad (9)$$

where a and b are the dimensions of the unit-cell, with respective values of 5.23×10^{-10} and 9.05×10^{-10} m; N_A denotes the Avogadro's number (6.022×10^{23} molecules/mol); MW is approximately 0.735 kg/mol, which represents the molecular weight of montmorillonite; and n_c is the number of TOT layers stacked per particle. Saiyouri et al. (2004) observed that n_c commonly decreases with

the increase of water content, and they determined an average of 100 layers at suctions around 107 MPa in the soil particle for Na-montmorillonite. While under almost fully saturated conditions, the mean value of n_c per particle is reported to be 10 (Delage et al., 2006), which we also use in this study.

Meanwhile, the interlayer distance h_{inter} varies depending on factors such as water activity, the type of montmorillonite, the dry density of the specimen and cation type. Experimentally, h_{inter} can be determined based on X-ray diffraction (XRD) measurements of the basal spacing d_{001} (the sum of layer thickness and interlayer distance). For Na-montmorillonite, XRD patterns exhibit discernible spacings for 1-, 2-, and 3-layer hydrates, with transitional shifts occurring gradually as relative humidity increases (Ferrage et al., 2005). Kozaki et al. (1998) observed interlayer distances corresponding to 2- and 3-layer hydrates in sodium montmorillonite compacted at dry densities ranging from 1000 kg/m³ to 1800 kg/m³ and in contact with distilled water, as depicted in Fig. 2 based on XRD findings.

It should be noted that, in addition to dry density, the XRD profiles also change as montmorillonite content changes, as evidenced by Wang et al. (2022). This indicates that the interlayer distance is influenced by both dry density and montmorillonite content. Therefore, following the method outlined in Muurinen et al. (2007), the interlayer distance is expressed as a function of the partial dry density of montmorillonite in the bentonite specimen (Fig. 3). Although the interlayer distance actually increases in a stepwise manner as the partial dry density of montmorillonite decreases, the linear relationship still shows good agreement with the experimental data from XRD tests conducted by Muurinen et al. (2004), Kozaki et al. (1998), and Sánchez et al. (2008):

$$h_{inter} = 1.41 \times 10^{-9} - 4.9 \times 10^{-10} \rho_{partial} \quad (10)$$

where ρ_w represents the density of porewater (kg/m³); and $\rho_{partial}$ denotes the partial dry density of montmorillonite in bentonite materials (kg/m³), which is defined as the ratio of the mass of montmorillonite to the combined volume of montmorillonite and total pore space (Liu et al., 2003). For the pure montmorillonite sample, $\rho_{partial}$ is identical to the total dry density, while for

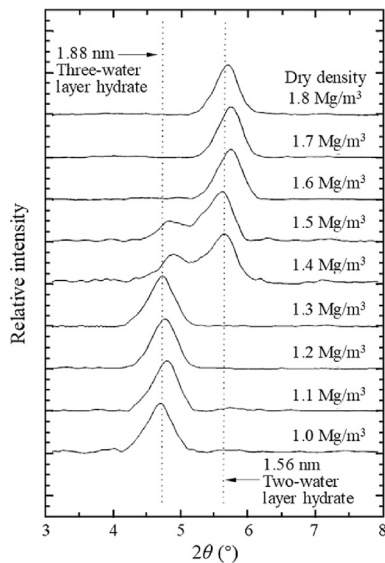


Fig. 2. XRD profiles for water-saturated Na-montmorillonite compacted at various dry densities (1 Mg/m³ = 1000 kg/m³) (data from Kozaki et al. (1998)).

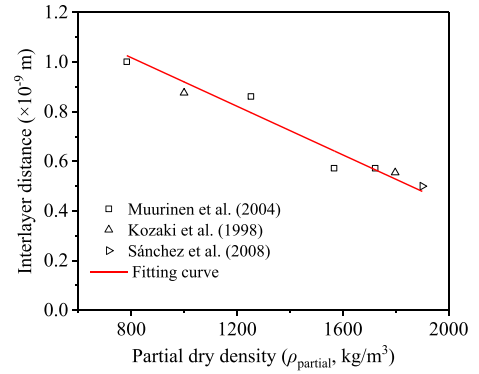


Fig. 3. Evolution of the interlayer distance with the partial dry density of montmorillonite within bentonite specimen.

bentonite materials containing non-montmorillonite particles, the $\rho_{partial}$ can be given by

$$\rho_{partial} = \frac{\rho_d \omega}{1 - (1 - \omega) \frac{\rho_d}{\rho_{nm}}} \quad (11)$$

where ρ_{nm} signifies the particle density (kg/m³) of constituent minerals other than montmorillonite within the bentonite.

Combining Eqs. (8)–(10), the interlayer porosities can be determined as

$$\eta_{inter} = \left(1.41 \times 10^{-9} - 4.9 \times 10^{-10} \frac{\rho_{partial}}{\rho_w} \right) \frac{ab(n_c - 1)}{n_c} \frac{N_A}{MW} \omega \rho_d \quad (12)$$

Fig. 4 illustrates the computed interlayer porosity results using Eq. (12) across various dry densities and mass fraction of montmorillonite in bentonite materials, assuming the bentonite particle density ρ_s of 2770 kg/m³. Curves in Fig. 4a show that an increase in the dry density initially leads to an increase in interlayer porosity, followed by a decreasing trend. Concurrently, at a specific dry density, the interlayer porosity consistently rises with an increase in the stacking interlayer number from 3 to 10 and the mass fraction of montmorillonite in bentonite clays. Since the interlayer porosity will not exceed the overall porosity of the specimen, the interlayer porosity curve will finally intersect with the overall porosity curve at a critical dry density. This critical dry density tends to increase with decreasing the amount of stacking TOT layers per particle at a given mass fraction of montmorillonite or with decreasing the mass fraction of montmorillonite at a given stacking number of TOT layers.

2.1.2. DDL and free porosity

The DDL is comprised of water molecules, cations, and anions, where an abundance of cations counteracts the charge on the outer surface of the montmorillonite. DDL water serves as the transitional region between the mineral surface and the free pore water. Calculation of the DDL porosity η_{DDL} , similar to that of interlayer volume, can be determined based on the external surface area and the thickness of DDL as follows:

$$\eta_{DDL} = A_{ext} h_{DDL} \omega \rho_d \quad (13)$$

where A_{ext} represents the external surface area of montmorillonite per unit mass (m²/kg), h_{DDL} represents the thickness of the DDL (m), and external surface area A_{ext} is comprised of the external basal surface area and the edge surface area. Therefore, the total external basal surface area can be calculated as follows:

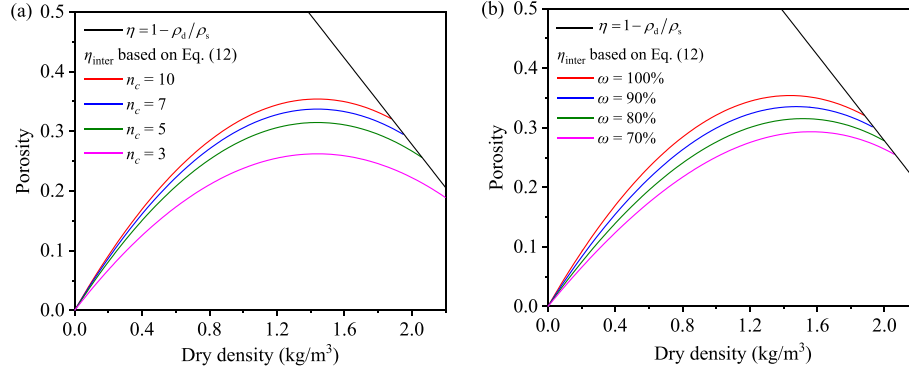


Fig. 4. Interlayer porosity in saturated bentonite with (a) different stacking numbers of n_c (with $\omega = 100\%$), and (b) different mass fractions of montmorillonite (with $n_c = 10$). Particle density of both montmorillonite and non-montmorillonite minerals is assumed to be 2770 kg/m^3 .

$$A_{\text{ext}} = 2 \frac{(n_a a)(n_b b) + (n_a a)(n_c c^*) + (n_b b)(n_c c^*)}{n_a n_b n_c} \quad (14)$$

where a , b , and c are the dimensions of montmorillonite unit-cell; and $c^* = c \sin 95^\circ$ is the orthogonally projected c -axis, d_{001} in XRD pattern and is equal to 0.96 nm . Commonly, the diameter of a montmorillonite TOT layer is about $50\text{--}200 \text{ nm}$ (Tournassat et al., 2011), which is much larger than its thickness of 0.96 nm . This implies that the stacking number in the direction of c -axis (n_c) is much less than that in the directions of a -axis (n_a) and b -axis (n_b). Consequently, the contribution of edge surface area to the total external surface is relatively small and can be neglected for simplicity. The A_{ext} in Eq. (14) then can be approximated by (Tournassat et al., 2011):

$$A_{\text{ext}} = 2 \frac{(n_a a)(n_b b)}{n_a n_b n_c} \frac{N_A}{MW} = \frac{2ab}{n_c} \frac{N_A}{MW} \quad (15)$$

Commonly, DDL exhibits a thickness on the nanometer scale, with its extent heavily influenced by ionic strength. This thickness can be quantified in terms of Debye lengths as follows:

$$h_{\text{DDL}} = \frac{3.09 \times 10^{-10}}{\sqrt{I}} f_{\text{DDL}} \quad (16)$$

where I represents the ionic strength (mol/L), and f_{DDL} denotes the number of Debye-lengths and is assumed to be 1 (Wu et al., 2018). The gas diffusion tests are usually conducted on bentonite saturated with deionized water (Sato et al., 2001; Higashihara et al., 2001, 2005). Komine and Ogata (1996) reported that the ion concentration of water surrounding compacted bentonite in contact with distilled water during swelling tests is approximately $0.02\text{--}0.04 \text{ mol/L}$, based on measurements from an ICP-atomic emission spectrometer. According to these experimental observations of ion concentration, a low ionic strength of 0.01 mol/L is employed for I in this study, which corresponds to a DDL thickness of 3.09 nm . By integrating Eqs. (13), (15) and (16), we can derive the DDL porosity η_{DDL} .

Note that, diffusion of neutral species, e.g. helium and hydrogen, being unaffected by the electrostatic potential generated by the negatively charged montmorillonite surfaces, contrasts with the diffusion of charged chemical species. The influence of DDL pores on gas diffusion is mainly due to the interaction between the gas molecule and external basal surface of montmorillonite. Within the DDL, pore regions near the external basal surface force gas diffusion pathways to align parallel to the basal surface, accompanied by a lower constrictivity value due to greater proximity to the basal

surface. In regions further from the external basal surface but still within the DDL zone, gas diffusion resembles that in free water pores and is less influenced by the TOT layer's external surface. To account for the limited impact of DDL pores on gas diffusion, we introduced a scaling factor χ to h_{DDL} in Eq. (16) which represents the reduced thickness affecting gas diffusion near the montmorillonite basal surface. Therefore, Eq. (16) can be rearranged as

$$h_{\text{DDL}} = \frac{3.09 \times 10^{-10}}{\sqrt{I}} f_{\text{DDL}} \chi \quad (17)$$

DDL porosity η_{DDL} then can be given as

$$\eta_{\text{DDL}} = 6.18 \times 10^{-10} \frac{ab}{n_c} \frac{N_A}{MW} \frac{1}{\sqrt{I}} f_{\text{DDL}} \chi \omega \rho_d \quad (18)$$

In water-saturated compacted bentonite, the total porosity is determined by summing the volumes of interlayer water, DDL water, and free water, then normalizing the result to the overall specimen volume. If the dry density of the bentonite ρ_d and the specific gravity of the soil particles ρ_s are provided, calculating the total porosity is straightforward:

$$\eta = 1 - \frac{\rho_d}{\rho_s} \quad (19)$$

Finally, substituting Eqs. (12), (18) and (19) into Eq. (5) yields the free porosity η_{free} as follows:

$$\eta_{\text{free}} = \left(1 - \frac{\rho_d}{\rho_s}\right) - \left(2.4\chi - 1.71 \frac{\rho_{\text{partial}}}{\rho_w} + 4.92\right) \times 10^{-4} \omega \rho_d \quad (20)$$

Fig. 5 shows the resulting DDL and free porosities for different scaling factors χ plotted against the dry density of a pure montmorillonite specimen, corresponding to $\omega = 100\%$. Obviously, both the η_{DDL} and η_{free} are very sensitive to scaling factor χ and show an opposite trend with increasing the dry density of specimen.

2.2. Estimation of the constrictivity and tortuosity

In water-saturated porous media, the gas diffusion process depends on the intermolecular collisions, e.g. water molecules-dissolved gas molecules. Constrictivity δ refers to the slowing of diffusion caused by increased viscosity in narrow pores due to the closer proximity of the diffusing particles to the average pore wall. This effect depends on both the pore diameter and the size of the diffusing particles, and becomes significant when the size of the gas

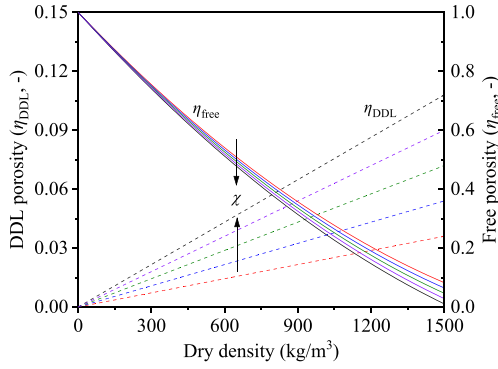


Fig. 5. Theoretical DDL and free porosities in pure montmorillonite specimen, shown as a function of scaling factor χ , ranging from 0.1 to 0.3 (increments of 0.05) increasing in the direction of the arrows. The solid and dashed lines represent η_{DDL} and η_{free} versus the specimen dry density, respectively.

molecules approaches the size of the pores $\lambda_p (<1)$. For quantification of the constrictivity parameter δ , empirical equations of power function (Beck and Schultz, 1970) and exponential function (Chantong and Massoth, 1983) have been proposed based on steady state and transient diffusion experiments of different solutes. However, a more generalized function developed by Renkin (1954) is widely accepted for evaluation of the pore constrictivity of porous medium:

$$\delta = (1 - \lambda_p)^2 (1 - 2.104\lambda_p + 2.09\lambda_p^3 - 0.95\lambda_p^5) \quad (21)$$

Here, by definition, δ_{free} is approximately equal to 1, as free water fills the macropores, which are significantly larger, ranging from tens of nanometers to micrometers, compared to the kinetic diameter of the gas molecule (0.289 nm for hydrogen gas and 0.26 nm for helium gas). For interlayer and DDL pores, λ_p can be determined based on Eqs. (10) and (17):

$$\lambda_{p_inter} = \frac{\text{kinetic diameter}}{1.41 \times 10^{-9} - 4.9 \times 10^{-10} \frac{\rho_{partial}}{\rho_w}} \quad (22)$$

$$\lambda_{p_DDL} = \frac{\text{kinetic diameter}}{3.09 \times 10^{-9} \chi} \quad (23)$$

where λ_{p_inter} and λ_{p_DDL} are the ratios of the gas molecule size to the size of interlayer and DDL pores, respectively. Finally, constrictivity for interlayer pores δ_{inter} and DDL pores δ_{DDL} can be obtained by substituting Eqs. (22) and (23) into Eq. (21), respectively. The constrictivity for interlayer pores is solely related to the partial

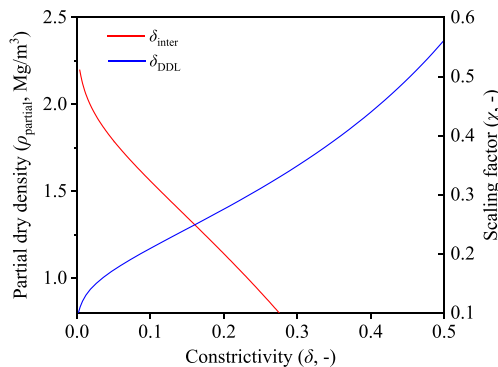


Fig. 6. Evolution of the constrictivity factor for both DDL and interlayer pores.

dry density of montmorillonite in bentonite materials, whereas for DDL pores, it is a variable dependent solely on the scaling factor. Fig. 6 shows the calculated constrictivity results for both the interlayer and DDL pores. Clearly, an increasing trend is observed for the constrictivity of interlayer pores δ_{inter} as $\rho_{partial}$ decreases. Meanwhile, regarding the constrictivity of DDL pores δ_{DDL} , there is a tendency for it to rise with an increase in the scaling factor.

For determining the τ^2 value, it is often assumed that diffusion pathways are primarily influenced by the basal surfaces of montmorillonite within the specimen, given that the average distance between two montmorillonite layers in a compacted bentonite is far below the diameter of a montmorillonite particle. Therefore, Kozaki et al. (2008) once proposed that the tortuosity parameter for free pores τ_{free}^2 is approximately equal to interlayer pores τ_{inter}^2 , due to the parallel nature of these two diffusion pathways. With the same reason, we further assume the relation $\tau_{DDL}^2 \approx \tau_{inter}^2$, leading to similar values among the three factors $\tau_{free}^2 \approx \tau_{inter}^2 \approx \tau_{DDL}^2$. Furthermore, increasing the dry density or further compacting the specimen primarily alters the relative proportions of the macropores to interlayer nanopores. However, the diffusion pathways still remain parallel or nearly parallel to the basal surfaces. Consequently, we assume that the tortuosity τ^2 of gas diffusion pathways remains relatively unchanged, which means that τ^2 can be regarded as a constant for compacted bentonite (Bourg et al., 2006). Based on experimental diffusion results on Na-montmorillonite (Sánchez et al., 2009; Suzuki et al., 2004) and Opalinus clay (Van Loon et al., 2004), and accounting for anisotropic effects at higher densities ($>1500 \text{ kg/m}^3$), Sánchez et al. (2009) derived a mean principal value for tortuosity of 12.8 ± 1.8 , corresponding to $11 < \tau^2 < 14.6$, which we adopted in this study regardless of the partial dry density of montmorillonite.

Finally, with the porosity η , constrictivity δ and tortuosity τ^2 parameters determined as mentioned above in the three types of porewater domains, Eq. (7) can be rearranged to calculate the D_a/D_w values as follows:

$$\frac{D_a}{D_w} = \frac{1}{\tau^2 \eta} (\eta_{free} + \delta_{DDL} \eta_{DDL} + \delta_{inter} \eta_{inter}) \quad (\tau^2 \in [11, 14.6]) \quad (24)$$

3. Experimental database

Several studies have reported on the apparent diffusion coefficients for hydrogen and helium gases in compacted, water-saturated Na-bentonite, including those by Eriksen and Jacobsson (1982), Neretnieks (1985), Sato et al. (2001), Higashihara et al. (2001, 2005), and Jacops et al. (2017). The experimental conditions are summarized in Table 1. Diffusion coefficients for helium and hydrogen gases were obtained using the through-diffusion or closed-cell methods.

The through-diffusion method employs the double through-diffusion approach, as described by Jacops et al. (2017). In this method, both sides of the bentonite specimen are connected to water vessels containing water and pressurized gas. Each compartment is filled with a different gas, such as helium and nitrogen, while maintaining equal total pressure to prevent any potential advective flux. Gas chromatography measures the change in gas composition over time in both reservoirs, allowing determination of the apparent diffusion coefficient through Fick's first law. On the other hand, the closed-cell method involves immersing a compacted water-saturated bentonite specimen in gas-saturated water within a sealed diffusion cell. After a specified duration, the bentonite specimen is sliced to analyse the new spatial distribution of gas concentration, facilitating the determination of the apparent

Table 1
Experimental database of reported measurements of gas diffusion in compacted water-saturated sodium bentonite.

Source	Gas type	Diameter of gas molecule (nm)	Bentonite type	Testing temperature	ω	ρ_s (Mg/m ³)	ρ_d (Mg/m ³)	ρ_{partial} (Mg/m ³)	D_w (m ² /s) ^c
Sato et al. (2001); Higashihara et al. (2005)	Helium gas	0.26	Kunipia-F	298 ± 0.1 K	1	2.77 ^b	0.8–1.6	0.8–1.6	7.5 × 10 ⁻⁹
Jacops et al. (2017)	Helium gas		MX-80	21 ± 2 °C	0.61	2.77	1.4	1.15 ± 0.09	7.5 × 10 ⁻⁹
Higashihara et al. (2001)	Hydrogen gas	0.289	Kunipia-F	298 ± 0.1 K	1	2.77	0.8–1.6	0.8–1.6	6.1 × 10 ⁻⁹
Eriksen and Jacobsson (1982); Neretnieks (1985)	Hydrogen gas		MX-80	25 °C	0.61	2.77	2	1.78 ± 0.08	6.1 × 10 ⁻⁹

^a Komine (2021) and Ruan et al. (2022).

^b Particle density of bentonite is calculated with the relation $\rho_s = \rho_m \rho_{\text{nm}} / [\omega \rho_{\text{nm}} + (1 - \omega) \rho_m]$, where ρ_m and ρ_{nm} are the densities of montmorillonite and non-montmorillonite minerals. ρ_m is assumed to be 2.77 Mg/m³ (Komine, 2008, 2021). For MX-80 bentonite, ρ_{nm} is also assumed to be 2.77 Mg/m³ for simplicity.

^c D_w values for helium and hydrogen gases in bulk water are obtained from Wise and Houghton (1966).

diffusion coefficient through Fick's second law (Higashihara et al., 2001).

Note that Table 1 presents gas diffusion data for two bentonite materials: Kunipia-F and MX-80. In Kunipia-F, where the montmorillonite content is nearly 100%, ρ_{partial} can be considered equal to the dry density of the specimen. In contrast, MX-80 is a highly variable material, with montmorillonite content ranging from approximately 61% (Ruan et al., 2022) to 80% (Komine, 2021), depending on the batch. This variability affects the partial dry density of montmorillonite in MX-80, potentially introducing errors in predicting the gas diffusion coefficient. To address this issue, error bounds have been included in the calculated ρ_{partial} value for MX-80 bentonite, as shown in Table 1 and the subsequent calculation results.

4. Results and discussion

4.1. Comparison between model prediction and experimental data

For prediction of D_a/D_w using Eq. (24), the parameters η_{inter} , η_{DDL} and η_{free} are determined by Eqs. (12), (18) and (20), respectively. The values for δ_{inter} and δ_{DDL} can be calculated based on Eq. (21), with δ_{free} set to 1. Additionally, a τ^2 value of 12.8 ± 1.8 is utilized for the three types porewater domains. As mentioned above, this value is a mean principal value of experimental results on Na-montmorillonite (Suzuki et al., 2004; Sánchez et al., 2009) and Opalinus clay (Van Loon et al., 2004), while also accounting for anisotropic effects. Utilizing the parameters of ω , ρ_s , ρ_d , and ρ_{partial} compiled in Table 1, we apply the least squares method to determine the scaling factor χ by fitting the experimental data of D_a/D_w to ρ_{partial} . Once the χ value is determined, the D_a/D_w can be calculated and compared with the experimentally measured values. Model predictions of D_a/D_w and the three types porewater porosities for helium and hydrogen gases are plotted against ρ_{partial} , as shown in Fig. 7a and c, respectively. The fitted parameters χ are almost equal for helium and hydrogen gases, with a value of 0.11 and 0.108, respectively. This is reasonable because the two type gases have similar kinetic molecule diameter and negligible adsorption on the montmorillonite layers, and diffusion processes of helium and hydrogen gases in bentonite are very similar. Meanwhile, the χ value of approximately 0.1 implies that only a very small portion (10%) of the total DDL porosity near the external basal surface influences the gas diffusion process, while the remaining 90% behaves similarly to free pore space. Overall, the model prediction results show good agreements with the experimental data for both the helium and hydrogen gases within the partial dry density of montmorillonite tested. The curves depicted in Fig. 7a and c illustrate that the D_a/D_w values for both helium and

hydrogen gases display a nearly linearly decreasing trend as ρ_{partial} increases. This phenomenon can be explained in terms of the porosity distribution and the resultant influence on the constrictivity of diffusion pathways. As shown in Fig. 7b and d, with the increase of ρ_{partial} , both the DDL and interlayer porosities show only slight changes, while a significant decrease of free porosity can be observed simultaneously. Moreover, an increase in ρ_{partial} will lead to a decrease in the constrictivity value of interlayer pores δ_{inter} (Fig. 6). These effects were then lumped into the proposed model (Eq. (23)), thus resulting in a decreasing trend of the D_a/D_w values.

However, in Fig. 7a and c, it is evident that the proposed model tends to underestimate the D_a/D_w values at ρ_{partial} below 900 kg/m³. This discrepancy between the predicted and measured D_a/D_w values could be explained in terms of the tortuosity parameter τ^2 . Tortuosity is related to the ratio of the actual travel path length to the length of the bentonite specimen. In this study, the τ^2 is assumed to be 12.8 ± 1.8 for the three types of porewater domains within the saturated bentonite specimen, irrespective of the partial dry density of montmorillonite ρ_{partial} . It is possible that the tortuosity parameter τ^2 decreases as the ρ_{partial} decreases. This phenomenon arises because decreasing the ρ_{partial} will induce a progressive increase in proportion of free water volume, where gas diffusion pathways are randomly distributed. However, the volume of interlayer and DDL water, where diffusion pathways could align parallel to the basal surfaces of montmorillonite tends to gradually decrease. Consequently, in pure water, where ρ_{partial} is decreased to 0 kg/m³ and there is an absence of montmorillonite particles, τ^2 is approximately equal to 1. This hypothesis is consistent with Bourg et al. (2006) who reported that the tortuosity for water tracers in Na-bentonite could increase rapidly when the ρ_{partial} remains at a lower level, such as for pure water or highly concentrated suspensions and dilute gels. Conversely, it exhibits negligible variation for concentrated gels and compacted bentonites. Based on the above analysis, we can combine Eq. (7) and the experimental values of the apparent diffusion coefficient (Fig. 7) to determine the optimal value of τ^2 for compacted, water-saturated bentonite:

$$\tau^2 = \frac{D_w}{D_a} \left(\frac{\eta_{\text{free}}}{\eta} + \delta_{\text{DDL}} \frac{\eta_{\text{DDL}}}{\eta} + \delta_{\text{inter}} \frac{\eta_{\text{inter}}}{\eta} \right) \quad (25)$$

Inserting the available values of D_a/D_w at $\rho_{\text{partial}} < 900$ kg/m³ into Eq. (25), we obtain τ^2 around 8 for both helium and hydrogen gases.

4.2. Effect of pore type domain on gas diffusion

Fig. 7b and d indicate that the free porosity shows more significant influence by the ρ_{partial} , than the DDL and interlayer porosities, decreasing rapidly to zero as ρ_{partial} approaches 1800 kg/m³. This ρ_{partial} value at free porosity of 0 aligns with the

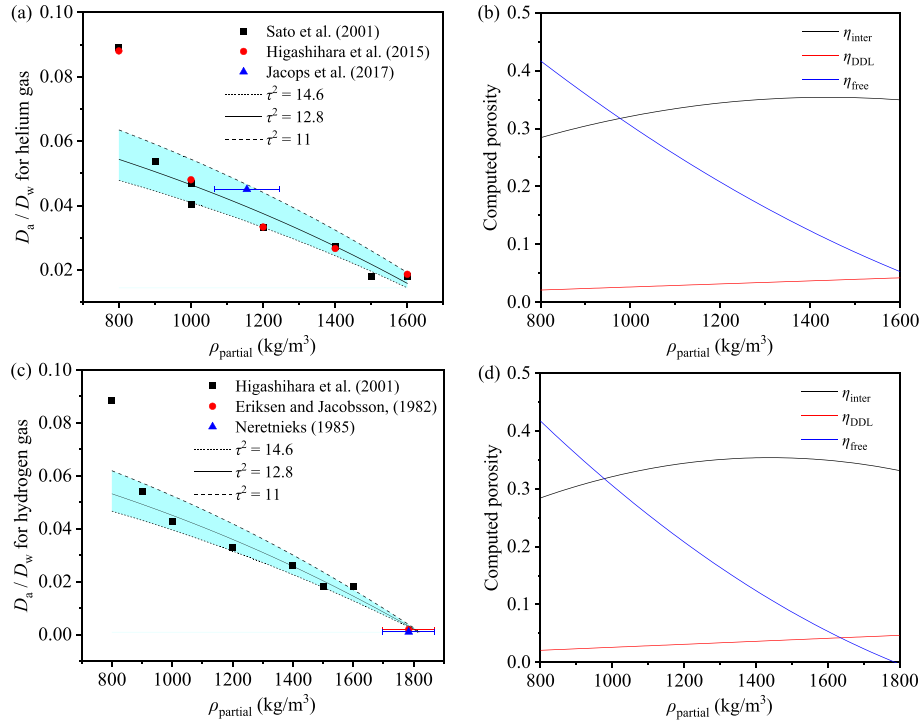


Fig. 7. Evolution of (a) D_a/D_w values and (b) calculated porosities for helium gas, along with (c) D_a/D_w values and (d) calculated porosities for hydrogen gas. The cyan regions indicate prediction ranges.

experimental results of Van Loon et al. (2007) and Wu et al. (2023). In Van Loon et al. (2007), anion diffusion tests were conducted on Volclay KWK bentonite (with a particle density of 2800 kg/m³ and a montmorillonite mass content of $\omega = 0.64$). Their measurements found η_{free} to be approximately 0.02–0.04 at a bulk dry density of 1900 kg/m³ ($\rho_{\text{partial}} \approx 1600$ kg/m³). Similarly, Wu et al. (2023) measured the diffusion coefficient of anions in Zhisin bentonite, which has a particle density of 2670 kg/m³ and a montmorillonite mass content of 0.368, reporting an η_{free} of 0.24 at a bulk dry density of 1800 kg/m³ ($\rho_{\text{partial}} \approx 1150$ kg/m³).

According to Eq. (24), the differences in gas diffusion coefficients among the interlayer, DDL, and free pore domains in saturated bentonite are governed not only by porosity but also by the constrictivity factor of each pore domain. The quantitative contributions of the three pore domains to the overall D_a/D_w values are calculated using the expression in Eq. (7): $\eta_i \delta_i / \tau^2 i \eta$, where i represents interlayer, DDL and free pore domains. Fig. 8 illustrates the calculated contributions of gas diffusion from each pore domain to the total D_a/D_w values. As shown in Fig. 8, gas diffusion in saturated

bentonite is predominantly controlled by the free pore domain for both helium and hydrogen gases, while the contributions from the DDL pores are nearly negligible. Although the interlayer pore is the dominant pore type, especially for ρ_{partial} values greater than 1000 kg/m³ (Fig. 7b and d), its contribution to the total D_a/D_w values remains relatively low due to significant constrictivity effects.

4.3. Comparison with predictions by Archie's law

In many cases, only the overall porosity of porous media can be determined, with pore size distribution and tortuosity remaining unknown. Therefore, the D_a/D_w values are typically determined by an empirical function of porosity alone, expressed as $D_a/D_w = \eta^m$, where m is an empirical exponent (Van Loon et al., 2007). This equation is derived analogously to Archie's law, an empirical correlation that describes electrical conductivity in sedimentary rocks. By extrapolating Archie's law, the dependence of D_a/D_w on the ρ_{partial} can be predicted by fitting the D_a/D_w values with the overall porosity. Fig. 9 illustrates the comparison of the predicted D_a/D_w

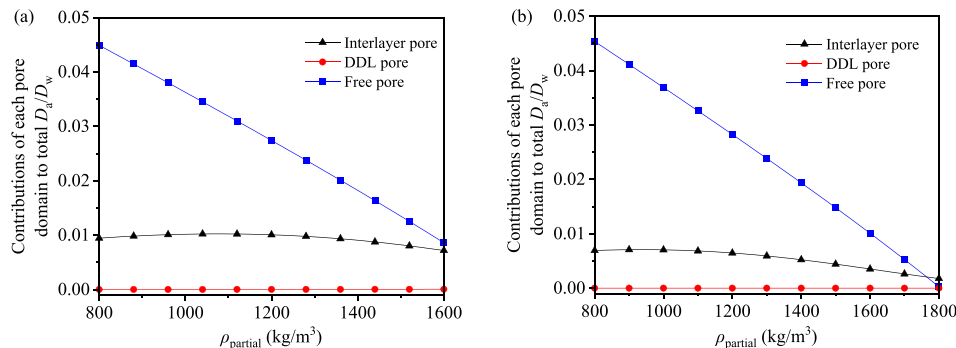


Fig. 8. Contributions of interlayer, DDL and free pore domains to the overall D_a/D_w values for (a) helium and (b) hydrogen gases.

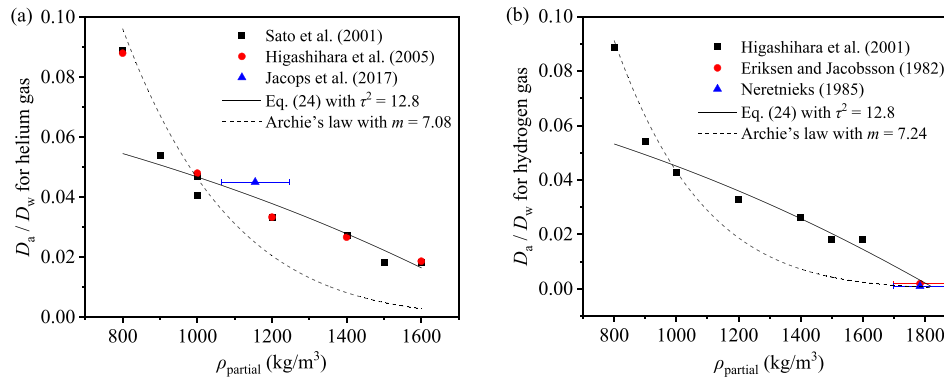


Fig. 9. Comparisons between the predicted D_a/D_w values by the proposed model (Eq. (24)) and those based on Archie's law for helium and hydrogen gases.

values between Archie's law and the proposed model in this study. The optimized values of the empirical exponent m in Archie's law are 7.08 and 7.24 for helium and hydrogen gases, respectively. It is evident that without separately evaluating the contributions of free pore, DDL pore and interlayer pore domains, Archie's law cannot provide adequate predictions for the diffusion coefficients of both helium and hydrogen gases. This is particularly noticeable for ρ_{partial} higher than 1000 kg/m^3 , as significant deviations between the measured data points and the predicted curve by Archie's law can be observed. This result emphasizes the importance of treating the three types of porewater domains within saturated compacted bentonite as individual and parallel processes, each with its unique geometric factors such as constrictivity and tortuosity. Generally, measuring the diffusion coefficient D_a/D_w is challenging due to the extended experimental duration. However, it can be predicted using the proposed model with knowledge of the physico-chemical properties of clay materials (bulk dry density, mass content of montmorillonite, internal and basal surface area, etc.) and geometric factors. The findings of this study mark a significant stride towards achieving a thorough comprehension of gas diffusion within compacted bentonite clays at pore scales.

5. Conclusions

The gas diffusion process in water-saturated Na-bentonite differs from that in bulk water due to the influence of the gas diffusion pathway length and the reduced mobility of dissolved gas molecules near the basal surface of montmorillonite layers. To address this, a new model was developed in this study, establishing a multiporosity system within saturated compacted bentonite materials, encompassing interlayer porosity, DDL porosity, and free porosity. Within this system, the apparent gas diffusion coefficient was quantified using weighted approximations based on individual porosities, tortuosity factor, and constrictivity factor in these three porosity domains. These parameters were determined based on the microstructure and crystallographic information of montmorillonite minerals.

The interlayer porosity was calculated according to the internal basal surface area of montmorillonite and the interlayer distance, while the DDL porosity was derived from the external basal surface area multiplied by the DDL thickness. The tortuosity factor was considered as a constant parameter of 12.8 ± 1.8 regardless of the bentonite specimen dry density, while the constrictivity factor was determined based on the relative size between the gas molecule diameter and the pore size. With these parameters obtained, the apparent diffusion coefficients of hydrogen and helium gases in water-saturated Na-bentonite materials can be calculated.

Verification results demonstrated that the model prediction results are in good agreement with the measured gas diffusion

coefficients for bentonite materials across a wide range of partial dry density of montmorillonite, i.e. 900 kg/m^3 to 1820 kg/m^3 , by employing only one fitting parameter, the scaling factor for the DDL thickness. However, as the partial dry density of montmorillonite decreases to 800 kg/m^3 , the proposed model tended to underestimate the apparent diffusion coefficient due to potential changes in the tortuosity factor. The newly proposed approach could provide a novel perspective for understanding the molecular diffusion of dissolved gas in bentonite materials.

CRedit authorship contribution statement

Linyong Cui: Writing – original draft, Validation, Methodology, Investigation, Conceptualization. **Min Chen:** Supervision, Resources, Formal analysis. **Zirui Cheng:** Writing – review & editing, Validation, Data curation. **Shakil A. Masum:** Writing – review & editing, Methodology, Data curation. **Yanan Cui:** Writing – review & editing, Validation, Investigation.

Declaration of competing interest

The authors declare that they have no known competing financial interests or personal relationships that could have appeared to influence the work reported in this paper.

Acknowledgments

The financial support from the National Natural Science Foundation of China (Grant No. 42202304) is greatly acknowledged.

References

- Appelo, C.A.J., Vinsot, A., Mettler, S., Wechner, S., 2008. Obtaining the porewater composition of a clay rock by modeling the in-and out-diffusion of anions and cations from an in-situ experiment. *J. Contam. Hydrol.* 101 (1–4), 67–76.
- Beck, R.E., Schultz, J.S., 1970. Hindered diffusion in microporous membranes with known pore geometry. *Science* 170 (3964), 1302–1305.
- Bourg, I.C., Sposito, G., Bourg, A., 2006. Tracer diffusion in compacted, water-saturated bentonite. *Clays Clay Miner.* 54 (3), 363–374.
- Bourg, I.C., Sposito, G., Bourg, A.C., 2007. Modelling cation diffusion in compacted water-saturated sodium bentonite at low ionic strength. *Environ. Sci. Technol.* 41 (23), 8118–8122.
- Boving, T.B., Grathwohl, P., 2001. Tracer diffusion coefficients in sedimentary rocks: correlation to porosity and hydraulic conductivity. *J. Contam. Hydrol.* 53 (1–2), 85–100.
- Chantong, A., Massoth, F.E., 1983. Restrictive diffusion in aluminas. *AIChE J.* 29 (5), 725–731.
- Chang, F.R.C., Skipper, N.T., Sposito, G., 1995. Computer simulation of interlayer molecular structure in sodium montmorillonite hydrates. *Langmuir* 11 (7), 2734–2741.
- Cui, L.Y., Masum, S.A., Ye, W.M., Thomas, H.R., Zhou, C., Hu, H.Q., 2024. Numerical investigation of gas migration behaviour in saturated bentonite with consideration of temperature. *Acta Geotech* 19, 2381–2393.
- Cui, L.Y., Ye, W.M., Wang, Q., Chen, Y.G., Cui, Y.J., 2023. A model for describing

- advective and diffusive gas transport through initially saturated bentonite with consideration of temperature. *Eng. Geol.* 107215
- Cui, L.Y., Ye, W.M., Wang, Q., Chen, Y.G., Chen, B., Cui, Y.J., 2022. Insights into gas migration in saturated GMZ bentonite using the RCP technique. *Eng. Geol.* 303, 106646.
- Cui, L.Y., Ye, W.M., Wang, Q., Chen, Y.G., Chen, B., Cui, Y.J., 2020. Insights into determination of gas breakthrough in saturated compacted Gaomiaozi bentonite. *J. Mater. Civ. Eng.* 32 (7), 04020190.
- Cui, L.Y., Ye, W.M., Wang, Q., Chen, Y.G., Chen, B., Cui, Y.J., 2019. Investigation on gas migration in saturated bentonite using the residual capillary pressure technique with consideration of temperature. *Process Saf. Environ. Prot.* 125, 269–278.
- Delage, P., Marcial, D., Cui, Y.J., Ruiz, X., 2006. Ageing effects in a compacted bentonite: a microstructure approach. *Geotechnique* 56 (5), 291–304.
- Eriksen, T.E., Jacobsson, A., 1982. Diffusion of Hydrogen, Hydrogen Sulfide and Large Molecular Weight Anions in Bentonite (No. SKBF-KBS-TR-82-17). Svensk Kaernbraenslefoersojning AB.
- Ferrage, E., Lanson, B., Sakharov, B.A., Drits, V.A., 2005. Investigation of smectite hydration properties by modeling experimental X-ray diffraction patterns: Part I. Montmorillonite hydration properties. *Am. Mineral.* 90 (8–9), 1358–1374.
- Geng, Z., Feng, Z., Li, H., Wang, Y., Wu, T., 2022. Porosity investigation of compacted bentonite using through-diffusion method and multi-porosity model. *Appl. Geochem.* 146, 105480.
- Higashihara, T., Otsuka, T., Sato, S., Ohashi, H., 2001. Diffusion of helium and estimated diffusion coefficients of hydrogen dissolved in water-saturated, compacted Ca-montmorillonite. *J. Nucl. Fuel Cycle Environ.* 7 (1), 51–55.
- Higashihara, T., Shibuya, H., Sato, S., Kozaki, T., 2005. Activation energy for diffusion of helium in water-saturated, compacted Na-montmorillonite. *Eng. Geol.* 81 (3), 365–370.
- Hueckel, T., Loret, B., Gajo, A., 2018. Expansive clays as two-phase, deformable, reactive continua: concepts and modeling options. In: *Chemo-mechanical Coupling in Clays: from Nano-Scale to Engineering Applications*. Routledge, pp. 105–120.
- Jacops, E., Maes, N., Bruggeman, C., Grade, A., 2017. Measuring diffusion coefficients of dissolved He and Ar in three potential clay host formations: boom Clay, Callovo-Oxfordian Clay and Opalinus Clay. *Geol. Soc. Spec. Publ.* 443 (1), 349–360.
- Kant, R., Prerna, 2022. Theory for diffusion: migration coupling-induced cathodic and anodic current anomaly. *J. Phys. Chem. C* 126 (45), 19035–19046.
- Komine, H., Ogata, N., 1996. Prediction for swelling characteristics of compacted bentonite. *Can. Geotech. J.* 33 (1), 11–22.
- Komine, H., 2008. Theoretical equations on hydraulic conductivities of bentonite-based buffer and backfill for underground disposal of radioactive wastes. *J. Geotech. Geoenviron. Eng.* 134 (4), 497–508.
- Komine, H., 2021. Cation filtration of montmorillonite on hydraulic conductivities of some bentonites in artificial seawater. *J. Geotech. Geoenviron. Eng.* 147 (5), 06021002.
- Kozaki, T., Fujishima, A., Sato, S., Ohashi, H., 1998. Self-diffusion of sodium ions in compacted sodium montmorillonite. *Nucl. Technol.* 121 (1), 63–69.
- Kozaki, T., Inada, K., Sato, S., Ohashi, H., 2001. Diffusion mechanism of chloride ions in sodium montmorillonite. *J. Contam. Hydrol.* 47 (2–4), 159–170.
- Kozaki, T., Liu, J., Sato, S., 2008. Diffusion mechanism of sodium ions in compacted montmorillonite under different NaCl concentration. *Phys. Chem. Earth* 33 (14–16), 957–961.
- Kumar, S., Chandane, A., Sengupta, A., Jayakrishnan, V.B., Sastry, P.U., Bajpai, R.K., 2023. Diffusion of Cs^+ in compacted Na^+/K^+ -saturated smectite-rich natural clay: role of clay microstructure. *J. Radioanal. Nucl. Chem.* 332 (1), 203–210.
- Liu, J., Kozaki, T., Horiuchi, Y., Sato, S., 2003. Microstructure of montmorillonite/silica sand mixture and its effects on the diffusion of strontium ions. *Appl. Clay Sci.* 23 (1–4), 89–95.
- Liu, J., Wang, Z., Guo, J., Jivkov, A., Sedighi, M., Shao, J., 2024. Gas migration at the granite–bentonite interface under semirigid boundary conditions in the context of high-level radioactive waste disposal. *Deep Undergr Sci Eng* 1–15.
- Liu, J.F., Guo, J.N., Ni, H.Y., Zhang, Q., Skoczylas, F., 2021. Swelling and gas transport characteristics of saturated compacted bentonite/sand samples considering the scale effect. *Geomech. Energy Environ.* 26, 100227.
- Liu, J.F., Ni, H.Y., Cao, X.L., Ma, L.K., Guo, J.N., Chen, X., 2020. Laboratory investigation on gas permeability of compacted GMZ bentonite under a coupled hydraulic-mechanical effect. *Eng. Geol.* 276, 105761.
- Marry, V., Turq, P., Cartailier, T., Levesque, D., 2002. Microscopic simulation of structure and dynamics of water and counterions in a monohydrated montmorillonite. *J. Chem. Phys.* 117 (7), 3454–3463.
- Muurinen, A., Karnland, O., Lehtikoinen, J., 2007. Effect of homogenization on the microstructure and exclusion of chloride in compacted bentonite. *Phys. Chem. Earth* 32 (1–7), 485–490.
- Muurinen, A., Karnland, O., Lehtikoinen, J., 2004. Ion concentration caused by an external solution into the porewater of compacted bentonite. *Phys. Chem. Earth* 29 (1), 119–127.
- Neretnieks, I., 1985. Diffusivities of some constituents in compacted wet bentonite clay and the impact on radionuclide migration in the buffer. *Nucl. Technol.* 71 (2), 458–470.
- Ni, H., Liu, J., Jivkov, A.P., Shen, W., Shao, J., 2023. A dual-porosity model for analysis of temperature effects on hydro-mechanical behaviour of GMZ bentonite under unconfined conditions. *Comput. Geotech.* 154, 105127.
- Radeisen, E., Shao, H., Hesser, J., Kolditz, O., Xu, W., Wang, W., 2023. Simulation of dilatancy-controlled gas migration processes in saturated bentonite using a coupled multiphase flow and elastoplastic H^2M model. *J. Rock Mech. Geotech. Eng.* 15 (4), 803–813.
- Renkin, E.M., 1954. Filtration, diffusion, and molecular sieving through porous cellulose membranes. *J. Gen. Physiol.* 38 (2), 225.
- Rotenberg, B., Marry, V., Vuilleumier, R., Malikova, N., Simon, C., Turq, P., 2007. Water and ions in clays: unraveling the interlayer/micropore exchange using molecular dynamics. *Geochem. Cosmochim. Acta* 71 (21), 5089–5101.
- Ruan, K., Wang, H., Komine, H., Ito, D., 2022. Experimental study for temperature effect on swelling pressures during saturation of bentonites. *Soils Found.* 62 (6), 101245.
- Saiyouri, N., Tessier, D., Hicher, P.Y., 2004. Experimental study of swelling in unsaturated compacted clays. *Clay Miner.* 39 (4), 469–479.
- Sánchez, F.G., Gimmi, T., Jurányi, F., Loon, L.V., Diamond, L.W., 2009. Linking the diffusion of water in compacted clays at two different time scales: tracer through-diffusion and quasielastic neutron scattering. *Environ. Sci. Technol.* 43 (10), 3487–3493.
- Sánchez, F.G., Van Loon, L.R., Gimmi, T., Jakob, A., Glaus, M.A., Diamond, L.W., 2008. Self-diffusion of water and its dependence on temperature and ionic strength in highly compacted montmorillonite, illite and kaolinite. *Appl. Geochem.* 23 (12), 3840–3851.
- Sato, S., Otsuka, T., Kuroda, Y., Higashihara, T., Ohashi, H., 2001. Diffusion of helium in water-saturated, compacted sodium montmorillonite. *J. Nucl. Sci. Technol.* 38 (7), 577–580.
- Schampera, B., Šolc, R., Tunega, D., Dultz, S., 2016. Experimental and molecular dynamics study on anion diffusion in organically modified bentonite. *Appl. Clay Sci.* 120, 91–100.
- Shackelford, C.D., Moore, S.M., 2013. Fickian diffusion of radionuclides for engineered containment barriers: diffusion coefficients, porosities, and complicating issues. *Eng. Geol.* 152 (1), 133–147.
- Sposito, G., Gupta, V.K., Bhattacharya, R.N., 1979. Foundation theories of solute transport in porous media: a critical review. *Adv. Water Resour.* 2, 59–68.
- Suzuki, S., Sato, H., Ishidera, T., Fujii, N., 2004. Study on anisotropy of effective diffusion coefficient and activation energy for deuterated water in compacted sodium bentonite. *J. Contam. Hydrol.* 68 (1–2), 23–37.
- Tournassat, C., Bizi, M., Braibant, G., Crouzet, C., 2011. Influence of montmorillonite tactoid size on Na-Ca cation exchange reactions. *J. Colloid Interface Sci.* 364 (2), 443–454.
- Van Loon, L.R., Glaus, M.A., Müller, W., 2007. Anion exclusion effects in compacted bentonites: towards a better understanding of anion diffusion. *Appl. Geochem.* 22 (11), 2536–2552.
- Van Loon, L.R., Soler, J.M., Müller, W., Bradbury, M.H., 2004. Anisotropic diffusion in layered argillaceous rocks: a case study with Opalinus Clay. *Environ. Sci. Technol.* 38 (21), 5721–5728.
- Wang, H., Ito, D., Shirakawabe, T., Ruan, K., Komine, H., 2022. On swelling behaviours of a bentonite under different water contents. *Geotechnique* 74 (1), 64–80.
- Watanabe, Y., Yokoyama, S., Shimbashi, M., Yamamoto, Y., Goto, T., 2023. Saturated hydraulic conductivity of compacted bentonite–sand mixtures before and after gas migration in artificial seawater. *J. Rock Mech. Geotech. Eng.* 15 (1), 216–226.
- Wise, D.L., Houghton, G., 1966. The diffusion coefficients of ten slightly soluble gases in water at 10–60 °C. *Chem. Eng. Sci.* 21 (11), 999–1010.
- Wu, T., Hong, Y., Shao, D., Zhao, J., Feng, Z., 2023. Experimental and modeling study of the diffusion path of Ce (III)-EDTA in compacted bentonite. *Chem. Geol.* 636, 121639.
- Wu, T., Wang, Z., Tong, Y., Wang, Y., Van Loon, L.R., 2018. Investigation of Re (VII) diffusion in bentonite by through-diffusion and modelling techniques. *Appl. Clay Sci.* 166, 223–229.



Linyong Cui obtained his PhD in Engineering Geology from Tongji University in 2021. He is currently a post-doctoral fellow at The Hong Kong Polytechnic University. His research interest primarily focuses on gas and water flow in low and ultra-low permeability materials, as well as the thermal-hydraulic-mechanical (T-H-M) behaviour of hydrate-bearing sediments.